J|A|C|S
ARTICLES
Published on Web 03/20/2007

# Gas-Phase Chemistry of Actinides Ions: New Insights into the Reaction of $UO^+$ and $UO^{2+}$ with Water

Maria del Carmen Michelini, Nino Russo,* and Emilia Sicilia

*Contribution from the Dipartimento di Chimica and Centro di Calcolo ad Alte Prestazioni per Elaborazioni Parallele e Distribuite-Centro d'Eccellenza MURST, Università della Calabria, I-87030 Arcavacata di Rende, Italy*

Received August 5, 2006; E-mail: nrusso@unical.it

***Abstract:*** The ability of uranium monoxide cations, $UO^+$ and $UO^{2+}$, to activate the O−H bond of $H_2O$ was studied by using two different approaches of the density functional theory. First, relativistic small-core pseudopotentials were used together with B3LYP hybrid functional. In addition, frozen-core PW91−PW91 calculations were performed within the ZORA approximation. A close description of the reaction mechanisms leading to two different reaction products is presented, including all the involved minima and transition states. Different possible spin states were considered as well as the effect of spin−orbit interactions on the transition state barrier heights. The nature of the chemical bonding of the key minima and transition states was studied by using topological methodologies (ELF, AIM). The obtained results are compared with experimental data, as well as with previous studies on the reaction of the bare uranium cations with water, to analyze the influence of the oxo-ligand in reactivity.

## Introduction

Uranium is a central element in actinide chemistry because of its importance in the treatment of nuclear waste. The radioactive waste contains a significant amount of actinides with long half-lives that are difficult to treat in a safe and cost-effective manner using presently available technology. To identify improved remediation strategies, our knowledge of the chemical and physical properties of actinide compounds must be advanced. As a consequence, theoretical studies capable of making reliable predictions of the properties of actinide compounds are of main importance. The current interest in gas-phase actinides chemistry is proved by some recent reviews on the subject.[1]

The reaction products of gas-phase uranium and uranium monoxide cations with $H_2O$ have been studied by using different experimental techniques.[2−5] In particular, Jackson and collaborators[2] studied the reaction of $UO^+$ and $UO^{2+}$ with $H_2O$, using a quadrupole ion trap (QIT−MS) mass spectrometer. The reaction rate constants were determined by measuring the reaction rates at different partial pressures of the reagent gas. Schwarz et al. have analyzed the oxo ligand effect on the reactivity of $U^+$ in its reaction with different oxidizing reagents basing on fourier transform ion cyclotron mass spectrometry (FTICR−MS) experiments.[4] More recently, the oxidation reaction of dipositive actinide ions with different oxidants were performed by Gibson and collaborators, by means of FTICR−MS experiments.[5] In the case of the reaction between $UO^+$ and $H_2O$, the following reaction products were detected:[2]

$$UO^+ + H_2O \rightarrow UO_2^+ + H_2 \quad (1)$$

$$UO^+ + H_2O \rightarrow UO_2H^+ + H \quad (2)$$

Experimental results indicate that both reactions are exothermic. The reaction between $UO^+$ and water was found to proceed at a rate of $1.5 \pm 1 \times 10^{-11}$ $cm^3s^{-1}$ and showed a branching ratio of approximately 1:1,[2] in agreement with earlier experimental studies.[3] In contrast, in FTICR−MS experiments, the formation of $UO_2H^+$ was not observed.[4] Different experimental works[1b,5,6] have demonstrated that QIT−MS/FTICR−MS contrasting results are consequence of the different pressures used in the two techniques ($10^{-6}$ Torr for FTICR−MS, $10^{-3}$ Torr in the case of QIT−MS experiments). FTICR−MS conditions results, therefore, in bimolecular processes in contrast to QIT−MS, which results in three-body processes.

For the reaction of the doubled charged cation and water, similar reaction products

$$UO^{2+} + H_2O \rightarrow UO_2^{2+} + H_2 \quad (3)$$

$$UO^{2+} + H_2O \rightarrow UO_2H^{2+} + H \quad (4)$$

were not observed at the conditions of the experiments. Considering that the oxidation of $UO^{2+}$ by $O_2$ is an exothermic process,[2,4,5] and taking into account the O−O and $H_2$−O BDE

(1) (a) Gibson, J. K. *Int. J. Mass Spectrom.* **2002**, *214*, 1. (b) Gibson, J. K.; Marçalo, J. *Coord. Chem. Rev.* **2006**, *250*, 776.
(2) Jackson, G. P.; King, F. L.; Goeringer, D. E.; Duckworth, D. C. *J. Phys. Chem. A* **2002**, *106*, 7788. (Correction: Jackson, G. P.; King, F. L.; Goeringer, D. E.; Duckworth, D. C. *J. Phys. Chem. A* **2004**, *108*, 2139.)
(3) Armentrout, P. B.; Beauchamp, J. L. *Chem. Phys.* **1980**, *50*, 27.
(4) Cornehl, H. H.; Wesendrup, R.; Diefenbach, M.; Schwarz, H. *Chem.−Eur. J.* **1997**, *3*, 1083.
(5) Gibson, J. K.; Haire, R. G.; Santos, M.; Marçalo, J.; Pires de Matos, A. *J. Phys. Chem. A* **2005**, *109*, 2768.
(6) Jackson, G. P.; Gibson, J. K.; Duckworth, D. C. *Int. J. Mass Spectrom.* **2002**, *220*, 419.

10.1021/ja065683i CCC: $37.00 

***Table 1.*** Theoretical and Experimental Bond Dissociation Energies (in kJ/mol) for Mono- and Dicationic Uranium Oxides[a]

| method | $U–O^+$ ($^4\Delta$)[b] | $U–O^{2+}$ ($^3\Sigma_g$)[b] | $OU–O^+$ ($^2\Phi_u$)[c] | $OU–O^{2+}$ ($^1\Sigma_g$)[c] |
|---|---|---|---|---|
| B3LYP/SDD | 674.8 (1.794) | 594.2 (1.753) | 742.7 (1.760) | 478.3 (1.700) |
| PW91/ZORA | 879.5 (1.783) | 774.8 (1.753) | 868.7 (1.773) | 669.7 (1.719) |
| CASPT2 | 728.62[d] | – | – | – |
| experimental | 803 ± 25[e] 774 ± 17[g] | 690 ± 60[f] | 772 ± 56[e] | 560 ± 30[f] |

[a] U−O bond lengths (in Å) are given in parentheses. [b] BDE calculated for the following dissociation process (all the species in their GS): $UO^{+(2+)} \rightarrow U^{+(2+)} + O$. [c] BDE calculated for the following dissociation process (all the species in their GS): $UO_2^{+(2+)} \rightarrow UO^{+(2+)} + O$. [d] Reference 20 (Spin−orbit result including basis set superposition error correction). [e] Data taken from ref 1(b). [f] Reference 5. [g] Reference 21.

***Table 2.*** First and Second Adiabatic Ionization Potentials (IP1, IP2, in eV), for UO and $UO_2$

| | UO | | $UO_2$ | |
|---|---|---|---|---|
| method | IP1 | IP2 | IP1 | IP2 |
| B3LYP/SDD | 6.70 | 12.58 | 6.29 | 15.32 |
| PW91/ZORA | 6.39 | 12.74 | 6.22 | 14.86 |
| experimental | 6.03[a] | 12.7 ± 0.8[b] | 6.13[a] | 14.6 ± 0.4[b] |

[a] Precise values: 6.0313 ± 0.0006 and 6.128 ± 0.003 eV, respectively (ref 22). [b] Reference 5.

(bond dissociation energies) values, it is possible to conclude that reaction 3 should be an exothermic process and that the reason for the lack of detection of reactivity is the slowness of the reaction.

In a recent paper, we have studied the interaction of $U^+$ and $U^{2+}$ with $H_2O$,[7] and we have found that in both reactions the dehydrogenation process is thermodynamically favored. The exothermic formation of $H_2$ from the reaction of $U^+$ and $H_2O$ evolves along a single spin surface, namely, the quartet spin state, which is the ground state (GS) of the bare cation. The reaction of $U^{2+}$ with water is less favored, both thermodynamically and kinetically, and presents a spin transition between the quintet and triplet spin surfaces.

The focus of this study involving uranium monoxide cations is to assess their ability to activate the O−H bond of water by getting a close description of the reaction mechanisms. In addition, we compare their reactivity patterns with experimental data as well as with the bare cations reactions, to asses the influence in reactivity produced by the addition of the oxygen ligand. It is a well-known fact that all f-elements have as a common feature a high oxophilicity, so it is interesting to evaluate the effect of oxo-ligands on the reactivity patterns of the metal center.[4]

For both studied reactions, we have considered two different spin states. Previous theoretical works have shown that dehydrogenation reactions involving first- and second-row transition metal cations usually involve more than one spin state.[8] This kind of behavior, in which more than one spin surface connects the reactants and products, is generally referred to as two-state reactivity.[9] In addition, in the case of actinides chemistry, a simplistic explanation for the observation that the formal spin may vary during a reaction without appreciably affect the rate is that weak spin−orbit coupling (Russel−Saunders coupling) does not apply to the heavy metal ions. Instead, strong spin−orbit coupling (*jj* coupling) better describes the electronic states and the requirement for spin conservation is thereby relaxed. Recent theoretical works involving gas-phase reactions of uranium atom with small molecules have shown the importance of taking into account different spin states.[10]

## Methodology and Computational Details

We have used two different approaches of density functional theory (DFT) to analyze the reactions under study. This choice was made based on our previous study of the bare cations reactivity.[7] First, DFT in its three-parameter hybrid B3LYP[11] formulation was used together with the Stuttgart basis set for the uranium atom (25s 16p 15d 7f)/[7s 6p 5d 3f] in combination with the 60 core electrons relativistic effective core potential (RECP).[12] This small-core RECP, so-called SDD pseudopotential, replaces the 60 electrons in inner shells 1−4, leaving the explicit treatment of the $n = 5$ shell (5s, 5p, 5d, and 5f), and also the 6s, 6p, 6d, and 7s valence electrons. Previous theoretical works have shown that the small-core RECP constitutes a good balance between the relativistic corrections introduced via the RECP and the explicit treatment of the valence electrons. The 6-311++G(d,p) basis set of Pople and co-workers was employed for the rest of the atoms[13] (we refer to these results as B3LYP/SDD, hereafter). These calculations were carried out with GAUSSIAN 2003 package.[14] "Ultra-fine" grids were adopted with the Gaussian program.

Further calculations were done using the ADF2004.01 software package.[15] The zero-order regular approximation (ZORA) was employed in ADF calculations. This approximation was used together with the PW91 functionals (exchange and correlation)[16] and a triple-$\zeta$ (TZ2P) basis sets (PW91/ZORA level, hereafter). We have used the frozen-core approach as implemented in ADF to describe the inner electrons of uranium. Therefore, for an uranium atom, all electrons up to 5d were considered as frozen; the remaining 14 electrons constituted the active valence shell.

Finally, single-point calculations were performed on the optimized geometries obtained at the PW91/ZORA level of

(7) Michelini, M. C.; Russo, N.; Sicilia, E. *Angew. Chem. Int. Ed.* **2006**, *45*, 1095.
(8) See, for instance, (a) Michelini, M. C.; Russo, N.; Sicilia, E. *J. Phys. Chem. A* **2002**, *106*, 8937. (b) Michelini, M. C.; Russo, N.; Sicilia, E.; Alikhani, M. E.; Silvi, B. *J. Phys. Chem. A* **2003**, *107*, 4862. (c) Chiodo, S.; Kondakova, O.; Michelini, M. C.; Russo, N.; Sicilia, E.; Irigoras, A.; Ugalde, J. M. *J. Phys. Chem.* **2004**, *108*, 1069. (d) Michelini, M. C.; Russo, N.; Sicilia, E. *Inorg. Chem.* **2004**, *43*, 4944. (e) Irigoras, A.; Elizalde, O.; Silanes, I.; Fowler, J. E.; Ugalde, J. M. *J. Am. Chem. Soc.* **2000**, *122*, 114, and references therein.
(9) (a) Schroder, D.; Shaik, S.; Schwarz, H. *Acc. Chem. Res.* **2000**, *33*, 139. (b) Armentrout, P. B.; Beauchamp, J. L. *Acc. Chem. Res*. **1989**, *22*, 315; (c) Poli, R.; Havey, J. N. *Chem. Soc. Rev.* **2003**, *32*, 1.
(10) (a) Gagliardi, L.; La Manna, G.; Roos, B. O. *Faraday Discuss.* **2003**, *124*, 63. (b) Balasubramanian, K.; Siekhaus, W. J.; McLean, W., II. *J. Chem. Phys.* **2003**, *119*, 5889.
(11) (a) Becke, A. D. *J. Chem. Phys.* **1993**, *98*, 5648. (b) Lee, C.; Yang, W.; Parr, R. G. *Phys. Rev. B* **1988**, *37*, 785.
(12) (a)http://www.theochem.unistuttgart.de/pseudopotentiale/. (b) Külchle, W.; Dolg, M.; Stoll, H.; Preuss, H. *J. Chem. Phys.* **1994**, *100*, 7535.
(13) (a) Krishnan, R.; Binkley, J. S.; Seeger, R.; Pople, J. A. *J. Chem. Phys.* **1980**, *72*, 650. (b) Blaudeau, J.-P.; McGrath, M. P.; Curtiss, L. A.; Radom, L. *J. Chem. Phys*. **1997**, *107*, 5016. (c) Clark, T.; Chandrasekhar, J.; Schleyer, P. V. R. *J. Chem. Phys*. **1983**, *74*, 294.
(14) Frisch, M. J.; et al. Gaussian 03, revision C.02, Gaussian, Inc.: Wallingford, CT, 2004.
(15) (a) te Velde, G.; Bickelhaupt, F. M.; van Gisbergen, S. J. A.; Fonseca Guerra, C.; Baerends, E. J.; Snijders, J. G.; Ziegler, T. *J. Comput. Chem*. **2001**, *22*, 931. (b) Fonseca Guerra, C.; Snijders, J. G.; te Velde, G.; Baerends, E. J. *Theor. Chem. Acc.* **1998**, *99*, 391. (c) ADF2004.01, SCM, Theoretical Chemistry, Vrije Universiteit, Amsterdam, The Netherlands, http://www.scm.com.

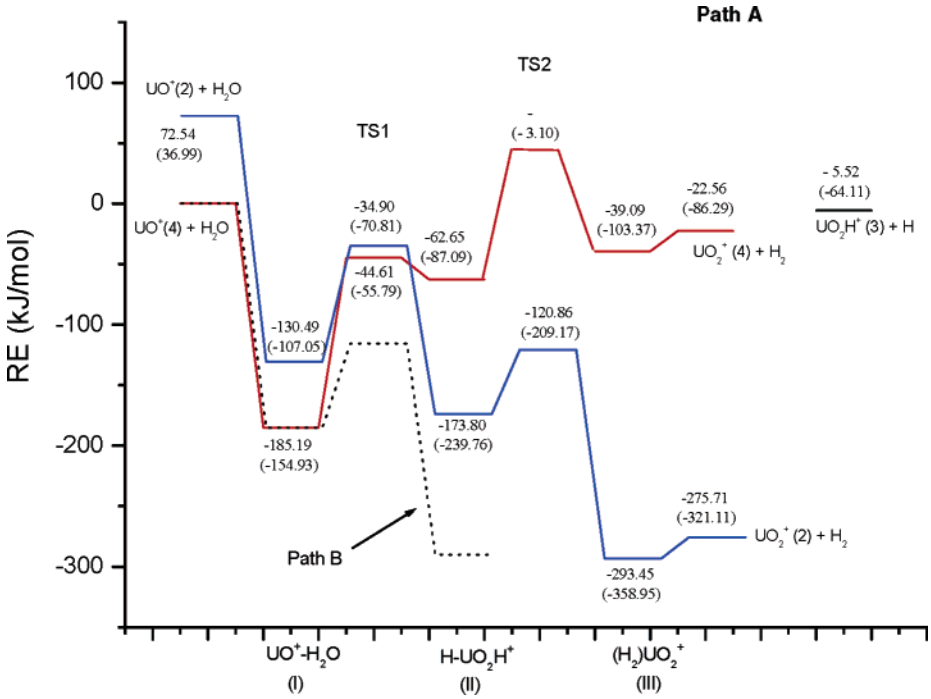


***Figure 1.*** Potential energy profiles for the reaction of $UO^+ + H_2O$ (Path A) at the B3LYP/SDD and PW91/ZORA levels of theory (in parentheses), corresponding to the quartet and doublet spin states. Spin multiplicities are given in parentheses.

***Table 3.*** Activation Barriers [kJ mol$^{-1}$] of the Transition States Involved in the Dehydrogenation Process (Path A)

| $UO^+$–$H_2O$ | B3LYP/SDD | PW91/ZORA | PW91/SO-ZORA |
|---|---|---|---|
| TS1[a] | 140.58 | 84.12 | 92.03 |
| TS2[b] | 52.94 | 30.59 | 33.48 |
| dissociation barrier[c] | 17.74 | 37.83 | 30.22 |
| $UO^{2+}$–$H_2O$ | B3LYP/SDD | PW91/ZORA | PW91/SO-ZORA |
| TS1′[a] | 312.78 | 232.85 | 242.37 |
| TS2′[b] | 130.24 | 81.28 | 76.84 |
| dissociation barrier[c] | 55.71 | 64.78 | 66.97 |

[a] Calculated as the energetic difference between the first transition state TS1 (TS1′) and the first complex I (I′). Due to the inverted stability order obtained at PW91/ZORA level for the TS1 moiety, at that level, this barrier corresponds to the difference between the TS1 ($^2$A), and the first complex (I) ($^4$A). [b] Calculated as the energetic difference between the second transition state TS2 (TS2′) and the first intermediate II (II′). In the case of the $UO^{2+}$ reaction, this difference has been calculated as the energetical difference between the TS2′ ($^1$A) and the H−$UO_2H^{2+}$ ($^3$A) at B3LYP/SDD level, whereas for the PW91/ZORA, the energetical difference between TS2′ ($^1$A) and H−$UO_2H^{2+}$ ($^1$A), which are the GS of these species at this level of theory, was used. [c] Energy difference between the dissociated products ($UO^+ + H_2$ or $UO^{2+} + H_2$) and the last intermediate III (III′).

***Table 4.*** Activation Barriers [kJ mol$^{-1}$] of the Transition States Involved in the Dehydrogenation Process (Path B)

| $UO^+$–$H_2O$ | B3LYP/SDD | PW91/ZORA | PW91/SO-ZORA |
|---|---|---|---|
| TS3[a] | 69.68 | 49.64 | 46.26 |
| TS5[b] | 251.09 | 190.67 | 184.01 |
| TS2[c] | 52.94 | 30.59 | 33.48 |
| dissociation barrier[d] | 17.74 | 37.83 | 30.22 |
| $UO^{2+}$–$H_2O$ | B3LYP/SDD | PW91/ZORA | PW91/SO-ZORA |
| TS3′[a] | 170.94 | 122.76 | 129.50 |
| TS5′[b] | 340.47 | 269.37 | 267.40 |
| TS2′[c] | 130.24 | 81.28 | 76.84 |
| dissociation barrier[d] | 55.71 | 64.78 | 66.97 |

[a] Calculated as the energetic difference between TS3 (TS3′) and the first complex I (I′). [b] Calculated as the energetic difference between TS5 (TS5′) and the bis-hydroxide moiety, IV (IV′). [c] Calculated as the energetic difference between the second transition state and the intermediate II (II′). In the case of the $UO^{2+}$ reaction, this difference has been calculated as the energetical difference between the TS2 ($^1$A) and the H−$UO_2H^{2+}$ ($^3$A) at B3LYP/SDD level whereas for the PW91/ZORA, the energetical difference between TS2 ($^1$A) and H−$UO_2H^{2+}$ ($^1$A) was used, that is the GS for this species at the PW91/ZORA level. [d] Energy difference between the dissociated products ($UO^+ + H_2$ or $UO^{2+} + H_2$) and the last intermediate III (III′).

theory by using the spin−orbit ZORA implementation of ADF package together with the non-collinear approximation (PW91/SO-ZORA).

Full geometry optimizations were performed at both B3LYP/SDD and PW91/ZORA levels, trying several initial geometries for each species.

The nature of the calculated stationary points was characterized by a vibrational analysis performed within the harmonic approximation. The zero-point vibrational energy corrections were included in all the reported relative energies. We have ensured that every transition state has only one imaginary frequency, and that this frequency connects reactants and products by means of IRC (intrinsic reaction coordinate) calculations.

Calculations on open-shell systems were performed using spin-unrestricted methods. Spin contamination was not serious in most of the cases, as the value of $<S^2>$ never exceeded 3.76 for quartet states and 2.05 for triplet states. We have detected a higher departure from the theoretical $<S^2>$ value in some doublet spin state species, which, however, never exceeded the

(16) (a) Burke, K.; Perdew, J. P.; Wang, Y. In *Electronic Density Functional Theory: Recent Progress and New Directions*; Dobson, J. F., Vignale, G., Das, M. P., Eds.; Plenum: New York, 1998. (b) Perdew, J. P In *Electronic Structure of Solid '91*; Ziesche, P., Eschrig, H., Eds.; Akademie Verlag: Berlin, 1991; p 11. (c) Perdew, J. P.; Burke, K.; Wang, Y. *Phys. Rev. B: Condens. Matter Mater. Phys.* **1996**, *54*, 16533. (d) Perdew, J. P.; Chevary, J. A.; Vosko, S. H.; Jackson, K. A.; Pederson, M. R.; Singh, D. J.; Fiolhais, C. *Phys. Rev. B: Condens. Matter Mater. Phys.* **1992**, *46*, 6671. (e) Perdew, J. P.; Chevary, J. A.; Vosko, S. H.; Jackson, K. A.; Pederson, M. R.; Singh, D. J.; Fiolhais, C. *Phys. Rev. B: Condens. Matter Mater. Phys.* **1993**, *48*, 4978.

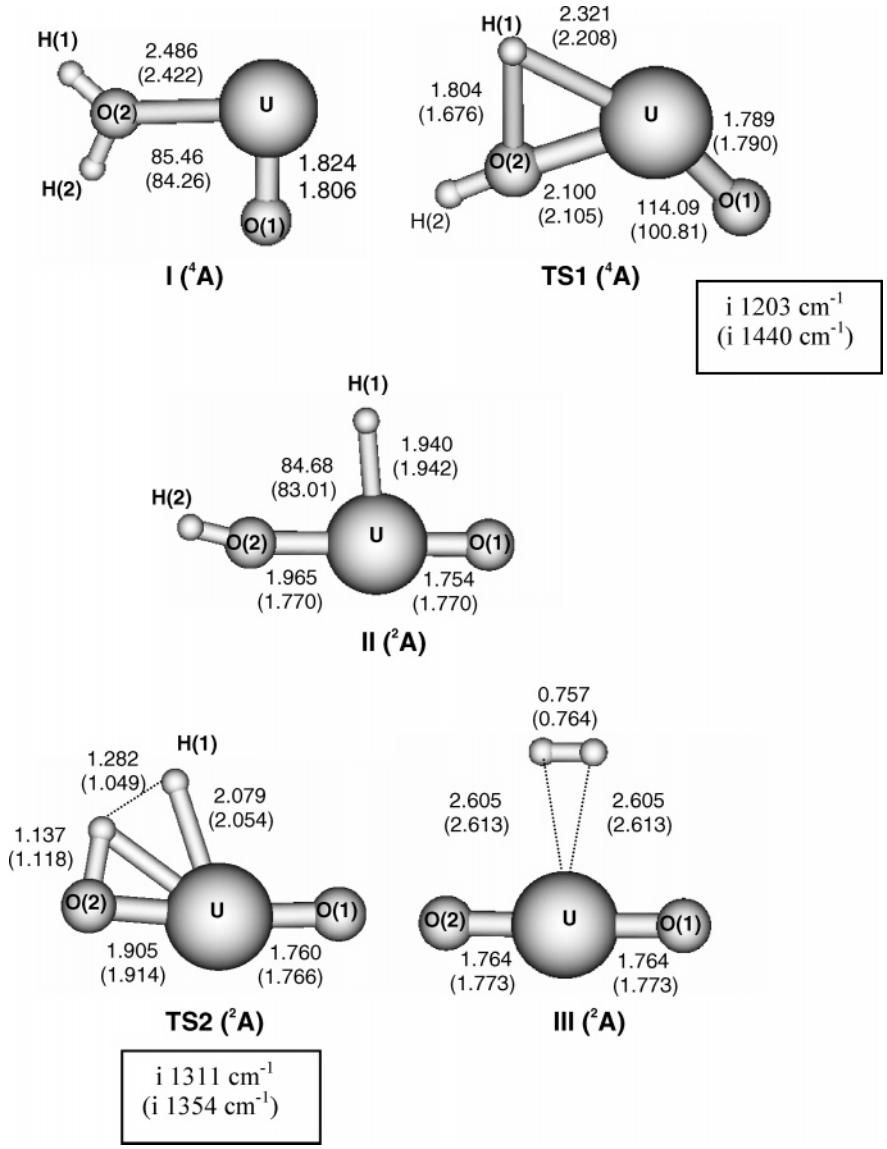


***Figure 2.*** Geometrical parameters of all the minima and transition states (lowest-energy spin state species) involved in the reaction of $UO^+$ with $H_2O$ (Path A), at the B3LYP/SDD and PW91/ZORA levels of theory (in parentheses). Bond lengths are in Ångstroms, and angles are in degrees.

value of 0.78 after annihilation of the first spin contaminant ($<S^2>_A$) (B3LYP/SDD calculations). To our knowledge, it is not possible to calculate that correction with ADF package; therefore, $<S^2>_A$ values are not reported at the PW91/ZORA level. It is worth noting that the spin contaminated species are not the ground state of the systems. We have also checked the stability of restricted closed-shell species (singlet state structures), and only in three cases a singlet−triplet instability was found. In all cases, the value of $<S^2>$ after annihilation of the first spin contaminant were lesser than 0.05. The details of $<S^2>$ and $<S^2>_A$ values for all the species reported in this work are included in the Supporting Information (Tables S14 and S15).

The characteristics of the bonding of all the key minima and transition states found along the reaction pathways were studied within the framework of topological metodologies. In particular, we have used the topological analysis of the electron localization function (ELF) as proposed by Silvi and Savin, by using TopMod package.[17]

Bonding and electronic properties were also explored using the atoms-in-molecules (AIM) techniques.[18] In particular, we have analyzed the main properties of the (3,−1) bond critical points (bcp) in the gradient field of the electron density. The bcps were primarily localized with the EXTREME program (part of the AIMPAC package)[18] and verified with TopMod program.

With the aim of comparison, atomic charges calculated within natural population analyses (NPA) and the bonding description provided by natural bond orbital (NBO) scheme were also performed.[19] The details of the bonding analyses are included in the Supporting Information, whereas here we present the main conclusions drawn from that study.

## Results and Discussion

We have first calculated the first and second adiabatic ionization potentials and the bond dissociation energies of the

(17) (a) Becke, A. D.; Edgecombe, K. E. *J. Chem. Phys.* **1990**, *92*, 5397. (b) Silvi, B.; Savin, A. *Nature* **1994**, *371*, 683. (c) Noury, S.; Krokidis, X.; Fuster, F.; Silvi, B. *TopMod Package*; Paris, 1997. (d) Noury, S.; Krokidis, X.; Fuster, F.; Silvi, B. *Comput. Chem.* **1999**, *23*, 597.
(18) Bader, R. F. *Atoms in molecules. A quantum theory*; Clarendon: Oxford, 1990.
(19) (a) Reed, A. E.; Weinhold, F. *J. Chem. Phys.* **1985**, *83*, 1736. (b) Reed, A. E.; Curtiss, L. A.; Weinhold, F. *Chem. Rev.* **1988**, *88*, 899.

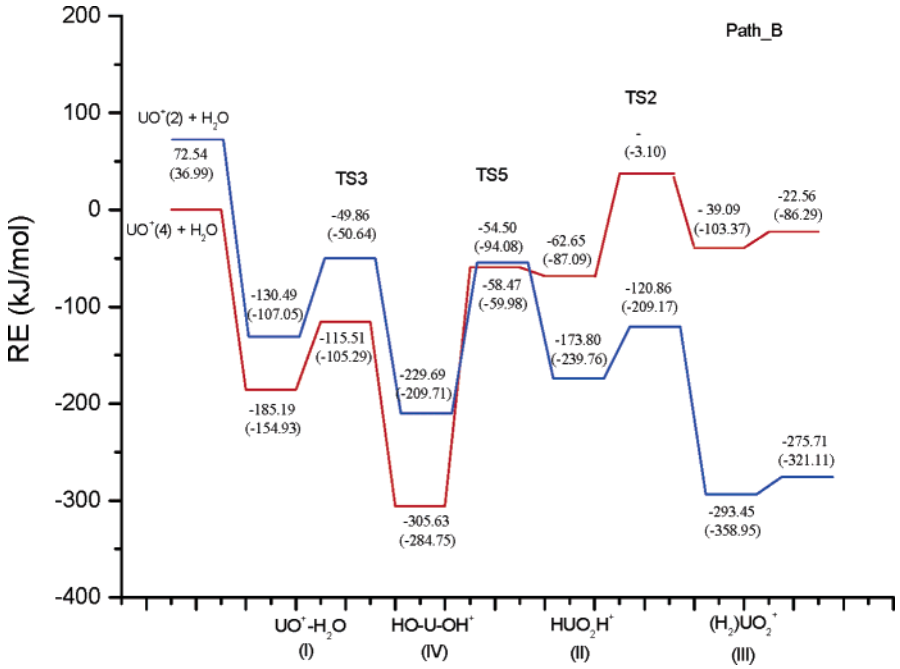


***Figure 3.*** Potential energy profiles for the reaction of $UO^+ + H_2O$ (Path B) at the B3LYP/SDD and PW91/ZORA levels of theory (in parentheses), corresponding to the quartet and doublet spin states. Spin multiplicities are given in parentheses.

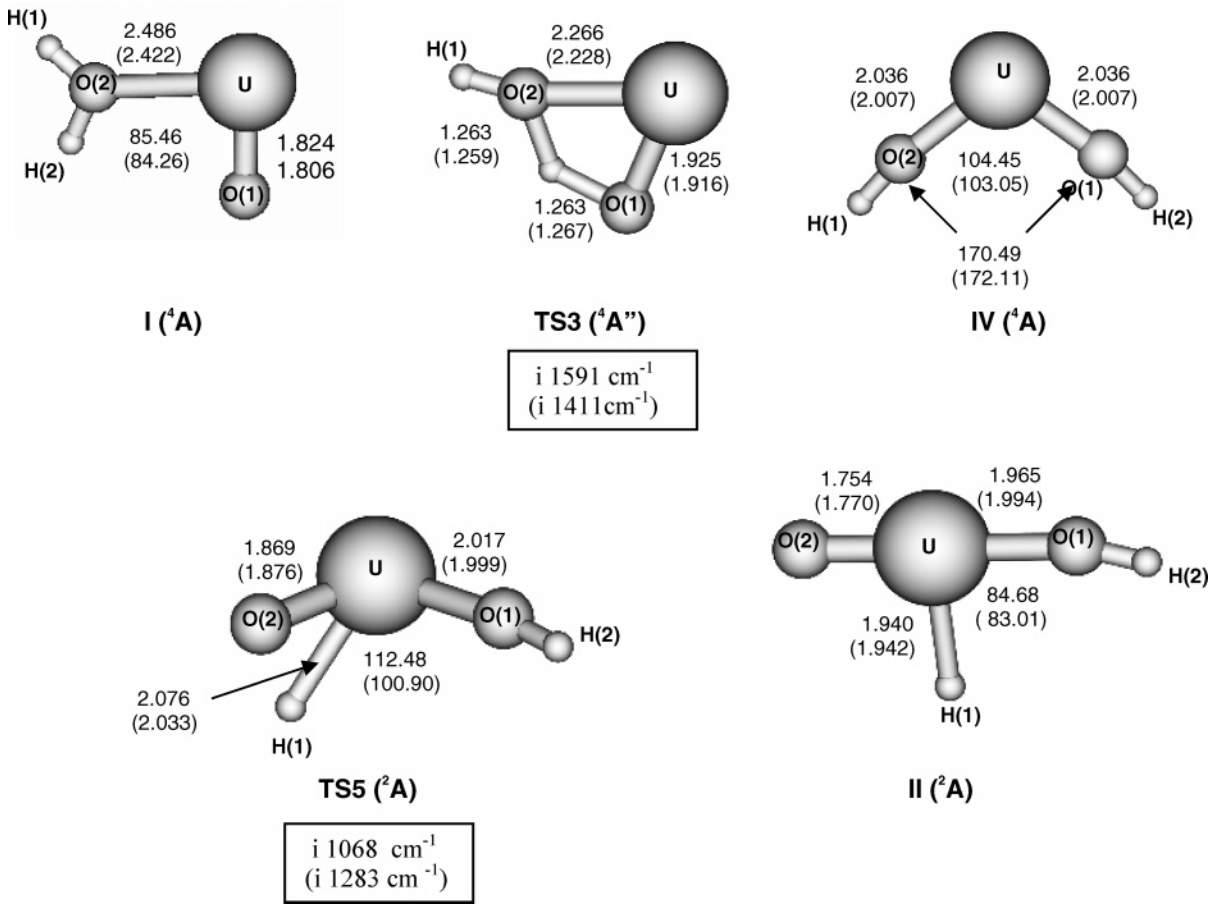


***Figure 4.*** Geometrical parameters of all the minima and transition states (lowest-energy spin state species) involved in the reaction of $UO^+$ with $H_2O$ (Path B), at the B3LYP/SDD and PW91/ZORA levels of theory (in parentheses). Bond lengths are in Ångstroms, and angles are in degrees.

studied uranium oxides. The results are collected in Tables 1 and 2 , together with the corresponding experimental data. In Table 1 are reported the bond dissociation energies for the mono and dicationic uranium oxides. As can be seen, the experimental BDEs are systematically underestimated by B3LYP/SDD results and overestimated at the PW91/ZORA level of theory. However, the B3LYP/SDD results are in most cases closer to the experimental values.

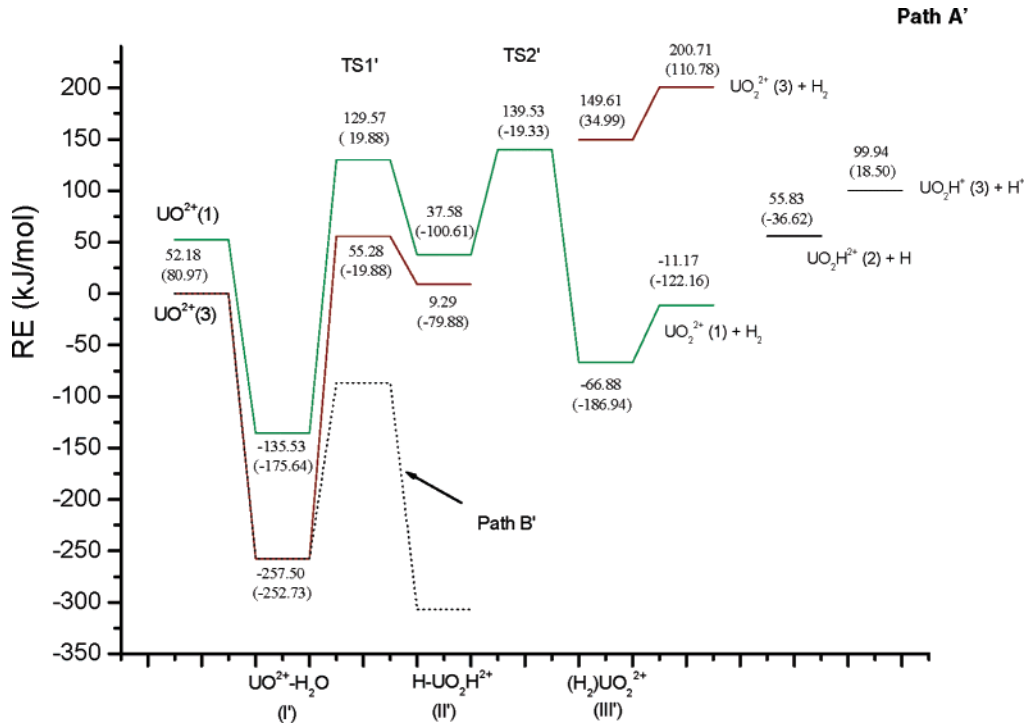


***Figure 5.*** Potential energy profiles for the reaction of $UO^{2+} + H_2O$ (Path A) at the B3LYP/SDD and PW91/ZORA levels of theory (in parentheses), corresponding to the quintet and triplet spin states. Spin multiplicities are given in parentheses.

In Table 2, we present the first and second adiabatic ionization potentials for UO and $UO_2$. In this case, the PW91/ZORA results are closer to the experimental data. From Tables 1 and 2, it can be concluded that the used levels of theory provide a reasonable agreement with the experimental values at a modest computational cost.

The dehydrogenation reaction is proposed to occur by a similar mechanism to the insertion mechanism for the bare cations.[7] This reaction mechanism, which is the most consistent with the experimental observations, involves the formation of an initial ion−dipole complex, followed by the O−H bond breaking that is realized through a first transition state, which corresponds to a hydrogen shift from the O atom to the metal center to form a hydrido-metal-hydroxy intermediate. After the formation of this intermediate, a second hydrogen migration from oxygen to uranium yields the second insertion intermediate. From this molecular structure, the reaction can proceed barrierless toward the dehydrogenation products. This reaction pathway, which involves two transition states, is called "Path A" hereafter. We have found a different reaction path (Path B), which shares with the previously described path A the entrance channel, i.e., the formation of the ion−molecule complex. However, instead to the transfer of a H atom to the metal atom, this mechanism involves a previous step in which the O−H bond breaking yields a bis-hydroxide intermediate, which is energetically very stable. The next step involves a transfer of an H atom from one of the OH groups to the metal atom, and from this point of the reaction, both reaction paths (A and B) follow an identical way. Path B, therefore, involves three different transition states.

The side product $UO_2H^+$ (or $UO_2H^{2+}$) can be formed by direct breaking of the hydrogen−uranium bond from the hydroxy-intermediate ($H-UO_2H^{+\ (2+)}$). In the case of the dicationic oxide, we have also considered the charge separation asymptote, $UO_2H^+ + H^+$.

In the following sections, the details of the potential energy surfaces (PESs) corresponding to the interaction of $UO^+$ and $UO^{2+}$ with water, for both, the ground and the lowest-lying excited state, are examined.

**$UO^+$ Insertion into O−H Bond.** In Figure 1, we present the first studied reaction pathway (Path A) for the interaction of $UO^+ + H_2O$. The spin states considered were the quartet spin state that is the ground state of the bare oxide cation and the doublet low-lying excited state.

As previously mentioned, the first step of the reaction involves the exothermic formation of a stable ion−dipole complex, $UO^+-H_2O$ (I). Different initial geometries were considered, and the one reported here, which is a planar structure, is the lowest energy structure.

The geometrical parameters of all the stationary points along the dehydrogenation pathway (Path A), for the ground spin state of each species at both levels of theory, are presented in Figure 2. The imaginary frequencies of all the transition structures are reported in the same figure.

As previously mentioned, in the first studied mechanism, the formation of the initial complex, $UO^+-H_2O$, is followed by the activation of the first O−H bond, leading the first insertion intermediate, $H-UO_2H^+$ (II). The formation of this insertion intermediate is possible after the system surpasses the first transition state (TS1), whose barrier height is of around 140 kJ/mol according to B3LYP/SDD calculations (84 kJ/mol at the PW91/ZORA level). In Table 3 are gathered the reaction barrier heights for the $UO^+ + H_2O$ reaction (path A), at all the studied levels of theory. The TS1 quartet and doublet spin states are quite close in energy at both levels of theory. It must be noted that the relative stability order is different depending on the level of theory. B3LYP/SDD calculations indicate the quartet spin state as the GS of this system, whereas the doublet state is the lowest energy structure at the PW91/ZORA level. It is evident, however, that

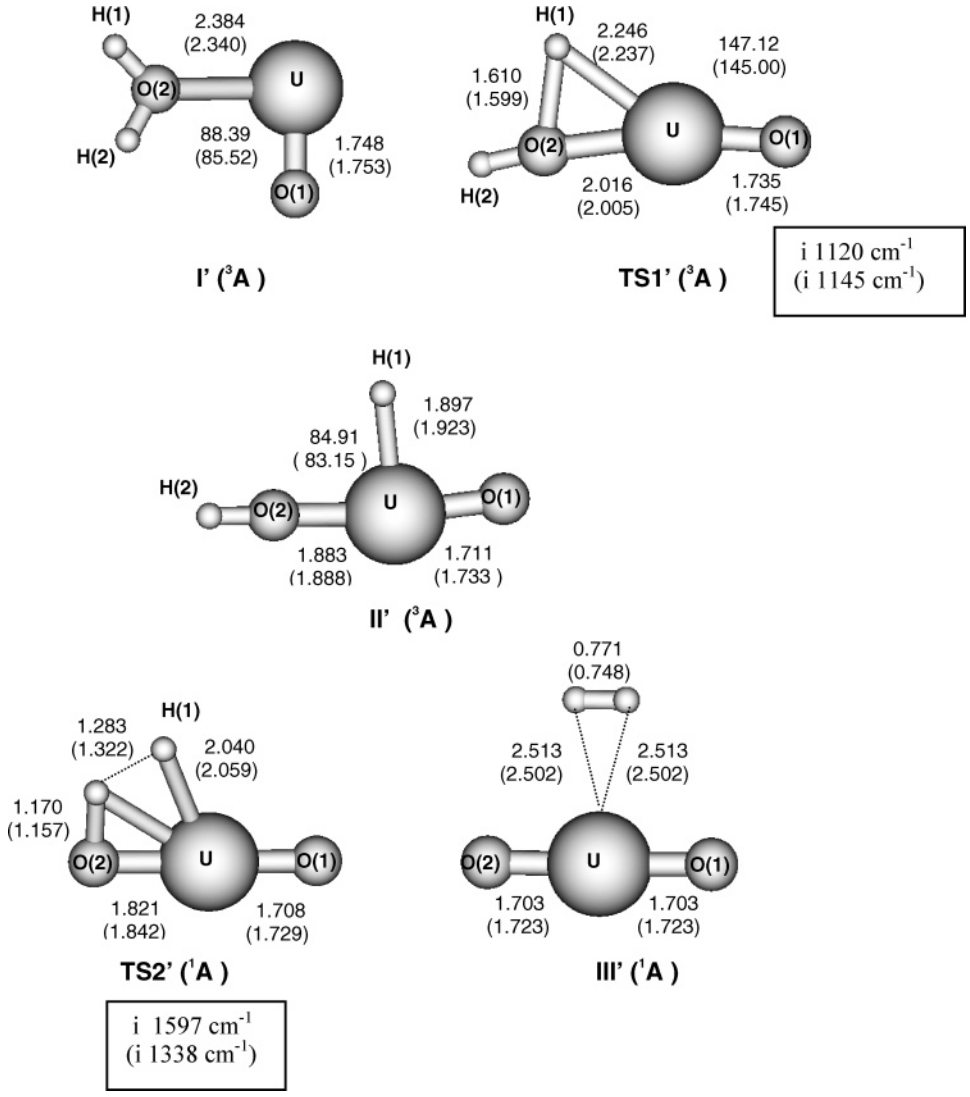


***Figure 6.*** Geometrical parameters of all the minima and transition states (lowest-energy spin state species) involved in the reaction of $UO^{2+}$ with $H_2O$ (Path A), at the B3LYP/SDD and PW91/ZORA levels of theory (in parentheses). Bond lengths are in Ångstroms, and angles are in degrees.

this region of the potential energy surface, between the first complex and the first insertion intermediate, is crucial because of the surmised crossing between the PESs. The rest of the reaction evolves along the doublet spin surface, at both levels of theory.

According to B3LYP/SDD results, the formation of the insertion intermediate is slightly less exothermic than the formation of the first complex, whereas at the PW91/ZORA level, this intermediate is much more stabilized with respect to the asymptote ($UO^+$ ($^4\Delta$) + $H_2O$).

From the insertion intermediate (II), the reductive elimination of $H_2$ proceeds through the formation of a molecular hydrogen complex, $(H_2)UO_2^+$ (III), after passing through the second transition state (TS2). The system has to overcome an energetic barrier of almost 53 kJ/mol according to our B3LYP/SDD calculations (31 kJ/mol at the PW91/ZORA level). The formation of the second insertion intermediate, $(H_2)UO_2^+$(III), is quite exothermic, namely, the energetic gain is of around 293 kJ/mol (359 kJ/mol at the PW91/ZORA level). The dihydrogen molecule is weakly bound as only 18 kJ/mol are required (38 kJ/mol at the PW91/ZORA) to form $UO_2^+$ ($^2\Phi_u$) + $H_2$, a process that is exothermic by 275.71 kJ/mol (B3LYP/SDD) overall.

In addition to the previously mentioned dehydrogenation path that involves the $(H_2)UO_2^+$ intermediate, we have also considered the possible formation of a dihydride-uranium oxo ion, $(H)_2UO_2^+$ intermediate. These isomers were found to be higher in energy with respect to the $(H_2)UO_2^+$ structures. We note, however, that it was not possible to localize these isomers for all the studied spin states. Therefore, a different reaction path involving an alternative $(H)_2UO_2^+$ intermediate structure was not further considered.

As can be seen in Figure 1, the second exit channel, namely the formation of $UO_2H^+$ (triplet spin state) with the loss of a H atom, was found to be much less exothermic than the dehydrogenation reaction.

The second studied mechanim (Path B) involves an initial transfer of a H atom to the second oxygen atom, i.e., the formation of a bis-hydroxide structure from the initial $UO^+$-$H_2O$ complex. The reaction profile is shown in Figure 3, whereas the geometrical parameters of the involved minima are collected in Figure 4. With the aim of clarity, we have also

included in that figure the initial complex $UO^+-H_2O$ (I) and the hydrido-metal-hydroxy intermediate that Path B shares with Path A.

The transfer of the first hydrogen atom is found to be possible after the system surpasses a transition state (TS3 in Figure 3) of almost 70 kJ/mol at the B3LYP/SDD level (50 kJ/mol at PW91/ZORA).

In Table 4 are gathered the reaction barrier heights for the $UO^+ + H_2O$ reaction (path B), at all the studied levels of theory.

After the formation of the bis-hydroxide $HO-U-OH^+$, which is very favored thermodynamically, a second transition state permits the transfer of a H atom from one of the O−H groups to the metal atom (TS5 in Figures 3 and 4). We note that this structure in the doublet spin state is nonplanar. We have found several isomers of that structure (at both spin states), which were quite close in energy, including a planar structure that was found to be 10 kJ/mol higher in energy. The activation barrier of this process is quite high (251.09 kJ/mol at the B3LYP/SDD level, 190.67 kJ/mol at the PW91/ZORA level). It is worthwhile to note that we have also considered other possible reaction pathways for the dehydrogenation reaction from the bis-hydroxide structure, without success. It seems that the system has necessarily to pass through the $H-UO_2H^+$ intermediate, in which a U−H bond is present to yield the $H_2$ elimination channel.

After the formation of the mono-hydroxide intermediate, $H-UO_2H^+$ (II), path B coincides with the previously described path A. In Table 4, we have included all the activation barriers of path B to give a complete view of the different steps followed by the system.

The geometrical parameters obtained at the B3LYP/SDD and PW91/ZORA levels are very close, with the major deviation being less than 0.2 Å for distances and 14° for angles.

**$UO^{+2}$ Insertion into O−H Bond.** The reaction between the double charged cation $UO^{2+}$ and $H_2O$ evolves along a reaction pathway similar to the previously described $UO^+$ reaction paths, namely, for Path A′, the initial formation of an ion−molecular complex (I′) is followed by the formation of an insertion intermediate $H-UO_2H^{2+}$ (II′), obtained after the system surmounts the first transition state (TS1′). Then, the $H-UO_2H^{2+}$ intermediate rearranges while passing through the second transition state, TS2′, to form the last intermediate $(H_2)UO_2^{2+}$ (III′).

The $UO^{2+} + H_2O$ reaction profile is depicted in Figure 5, whereas in Figure 6 we report the geometrical parameters for all the ground spin state species involved in this reaction.

As can be seen in Figure 5, the reaction profile shows a different trend of that of the reaction of $UO^+$ and $H_2O$. First, the formation of the first complex (I′), $UO^{2+}-H_2O$, is much more exothermic than the corresponding step for the reaction of $UO^+$, namely, the process is exothermic by as much as 257.50 kJ/mol at B3LYP/SDD (252.73 kJ/mol at PW91/ZORA levels). Second, the first transition state (TS1′) has a very high barrier height, almost 313 kJ/mol at the B3LYP/SDD level of theory (233 kJ/mol at the PW91/ZORA level), which is more than two times the corresponding barrier for the $UO^+ + H_2O$ reaction (see Table 3).

The first insertion intermediate, $H-UO_2H^{2+}$ (II′), is quite high in energy in comparison to the $UO^{2+}-H_2O$ complex. At the B3LYP/SDD level, the formation of this intermediate is an endothermical process. It must be noted that the lowest-energy spin state of this intermediate is inverted at the PW91/ZORA level, namely, the singlet state is the GS for the $H-UO_2H^{2+}$ (II′) intermediate. According to PW91/ZORA calculations, therefore, the crossing from the triplet spin surface of the reactants to the singlet spin surface of the products should take place before the formation of the first insertion intermediate (II′). In contrast, at the B3LYP/SDD level, the change of spin state probably takes place before the formation of the second transition state. Unfortunately, despite careful searches, TS2′ could not be located on the triplet spin surface. This structure is surely very high in energy, considering the energetical values of the connected minima. The barrier height between the triplet spin $H-UO_2H^{2+}$ (II′) intermediate and the singlet TS2′ is of around 130 kJ/mol at the B3LYP/SDD level, whereas for PW91/ZORA the corresponding value is 81.28 kJ/mol (considering in this case the transition from the singlet $H-UO_2H^{2+}$ (II′) intermediate to the singlet TS2′).

The formation of the second insertion intermediate (III′) is also much less exothermic than the corresponding step for the reaction of $UO^+$. This structure has a relative energy of almost 67 kJ/mol at the B3LYP/SDD level (187 kJ/mol at the PW91/ZORA level), with respect to the $UO^{2+}$ ($^3\Sigma_g$) + $H_2O$ asymptote. Loss of $H_2$ requires an additional 56 kJ/mol of energy (at B3LYP/SDD, 65 kJ/mol at the PW91/ZORA level) to form the ground-state products $UO_2^{2+}$ ($^1\Sigma_g$) + $H_2$. The dehydrogenation reaction has an exothermicity of 11.17 kJ/mol at the B3LYP/SDD level (122 kJ/mol at PW91/ZORA), with respect to the 275.70 kJ/mol at the B3LYP/SDD level (321.11 kJ/mol at PW91/ZORA) obtained for the formation of $UO_2^+ + H_2$ from $UO^+ + H_2O$. We have also taken into account the possible formation of a dihydride−uranium oxo ion, $(H)_2UO_2^{2+}$, intermediate. However, neither in this case is this structure energetically favored.

The second exit channel, reaction 4, as well as the production of the $UO_2H^+ + H^+$ asymptote were found to be less favored energetically (see Figure 5).

As for the reaction of $UO^+ + H_2O$, we have analyzed the formation of the $U(OH)_2^{2+}$, bis-hydroxide isomer from the first ion−molecule complex (Path B′). Also in this case, the formation of this isomer is highly favored energetically. The transfer of the first hydrogen atom from the water molecule to the second oxygen atom takes place after the surpass of an energetic barrier (TS3′ in Figures 7 and 8) of almost 171 kJ/mol at the B3LYP/SDD level of theory (123 kJ/mol at the PW91/ZORA level). After the formation of the $HO-U-OH^{2+}$ moiety, the system passes through a second transition state (TS5′), which produces the insertion intermediate $H-UO_2H^{2+}$, already described in path A. We note that up to the formation of the $H-UO_2H^{2+}$ moiety, the system is still on the triplet spin state surface. After the formation of this intermediate, the system evolves along the previously described path A′. All the energetic barriers that the system has to surpass along this pathway are collected in Table 4.

**Comparison Between the Theoretical Results.** Comparing the results obtained by the different DFT approaches used in this work, we note that in some cases the relative energies are notably different. We found the largest differences in the case of the $UO^{2+} + H_2O$ reaction, particularly for the singlet spin

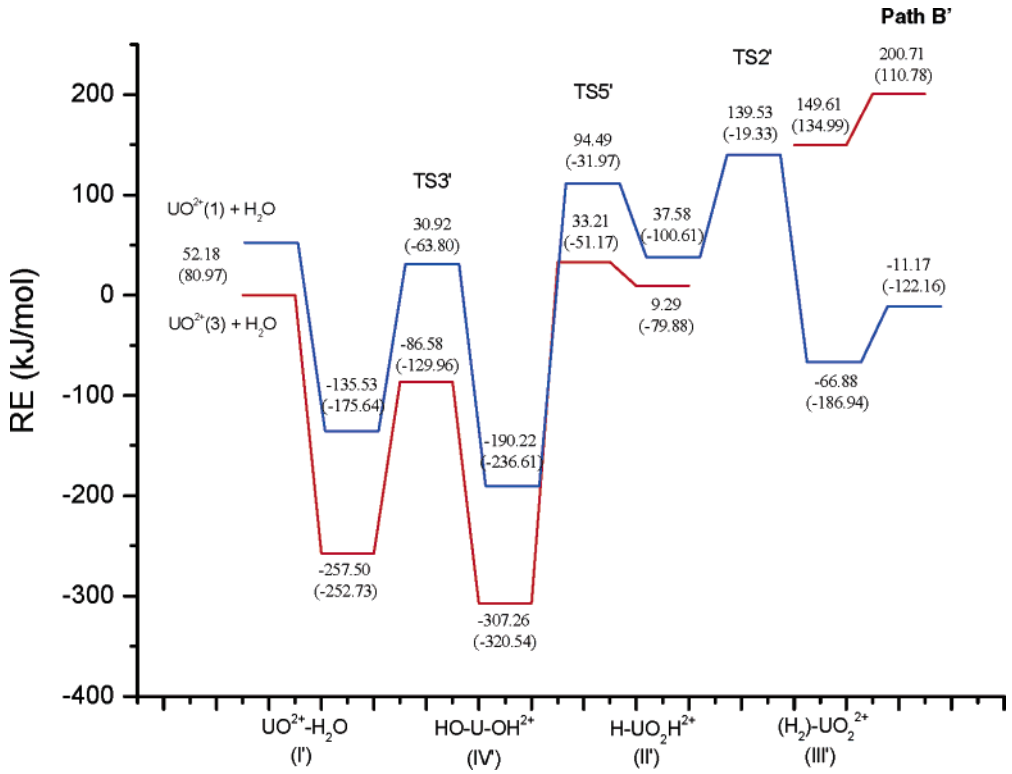


***Figure 7.*** Potential energy profiles for the reaction of $UO^{2+} + H_2O$ (Path B) at the B3LYP/SDD and PW91/ZORA levels of theory (in parentheses), corresponding to the quintet and triplet spin states. Spin multiplicities are given in parentheses.

state structures. In this section, we would like to underline some computational details that could give insight into the origin of that difference.

First, we note that in the case of B3LYP/SDD results, the small-core RECP replaces 60 electrons in the inner shells, leaving the explicit treatment of the remaining 30 electrons. In contrast, in the case of PW91/ZORA calculations, the active valence shell is constituted by only 14 electrons.

Second, we have to consider the different density functionals used in each approach. In our previous work,[7] we have studied the reactions of the bare uranium cations with water, by using three different DFT approaches, namely, in addition to the methods used in the present paper, we have also performed PW91/SDD calculations, with the aim to evaluate the effect of the change of functional on the results. We have noted that in the great majority of the cases, the results were systematically between the B3LYP/SDD and the PW91/ZORA results. Therefore, in that case, we could conclude that a significant part of the energetical differences was due to the different functional. We note in passing that the reason for the choice of a pure functional in the case of ZORA calculations is that hybrid functionals were fully implemented only in the last version of ADF package.

Third, in both methods, we have detected spin contamination in some of the structures, mainly in doublet spin states (see Supporting Information for details). The contamination was always comparable at both methodologies. In the case of the B3LYP/SDD calculations, the problem was solved after the annihilation of the first spin contaminant (Supporting Information, tables S14 and S15). To our knowledge, it is not possible to perform this type of correction with ADF program. For all the studied species, we have checked the wavefunction stability and performed the corresponding optimization each time that an instability was found. In this way, in the case of singlet spin states, for which we have found the most marked differencies between the approaches, we have checked the existence of singlet−triplet instabilities. This check was made only at the B3LYP/SDD level, because this option is not available in ADF code. In some cases, we have detected this type of instability (see Supporting Information). For these reasons, we consider that at least in the case of singlet and doublet spin states, B3LYP/SDD results are more reliable.

We remind the readers that the degree of spin contamination can be considered as an indication of the difficulties of DFT for correctly describe electronic structures that have some multireference character.[23] We have also to mention that several authors[24] have pointed out the wrong emphasis currently put into the use of the expectation value $<S^2>$ as a check of the reliability of unrestricted DFT (UDFT) results. In addition, due to the fact that UDFT indirectly actually covers some static electron correlation, in spite of its single-determinant nature,[24b] the existence of spin contamination is not a conclusive indication of the unreliability of UDFT results. We must underline, however, that due to the characteristics of the systems treated here, the only way to further test the performance of UDFT

(20) Paulovic, J.; Gagliardi, L.; Dyke, J. M.; Hirao, K. *J. Chem. Phys.* **2005**, *122*, 144317.
(21) Kaledin, L. A.; McCord, J. E.; Heaven, M. C. *J. Mol. Spectrosc.* **1994**, *164*, 27.
(22) (a) Han, J.; Kaledin, L. A.; Goncharov, V.; Komissarov, A. V.; Heaven, M. C. *J. Am. Chem. Soc.* **2003**, *125*, 7176. (b) Han, J.; Goncharov, V.; Kaledin, L. A.; Komissarov, A. V.; Heaven, M. C. *J. Chem. Phys.* **2004**, *120*, 5155.
(23) See for instance Jensen, K. P.; Roos, B. O.; Ryde, U. *J. Chem. Phys*. **2007**, *126*, 014103.
(24) (a) Gräfensten, J.; Kraka, E.; Filatov, M.; Cremer, D. *Int. J. Mol. Sci*. **2002**, *3*, 360. (b) Gräfensten, J.; Hjerpe, A. M.; Kraka, E.; Cremer, D. J. *Phys. Chem. A* **2000**, *104*, 1748. (c) Pople, J.; Gill, P. M. W.; Handy, N. C. *Int. J. Quant. Chem.* **1995**, *56*, 303. (d) Gräfensten, J.; Cremer, D. *Mol. Phys.* **2001**, *99*, 981.

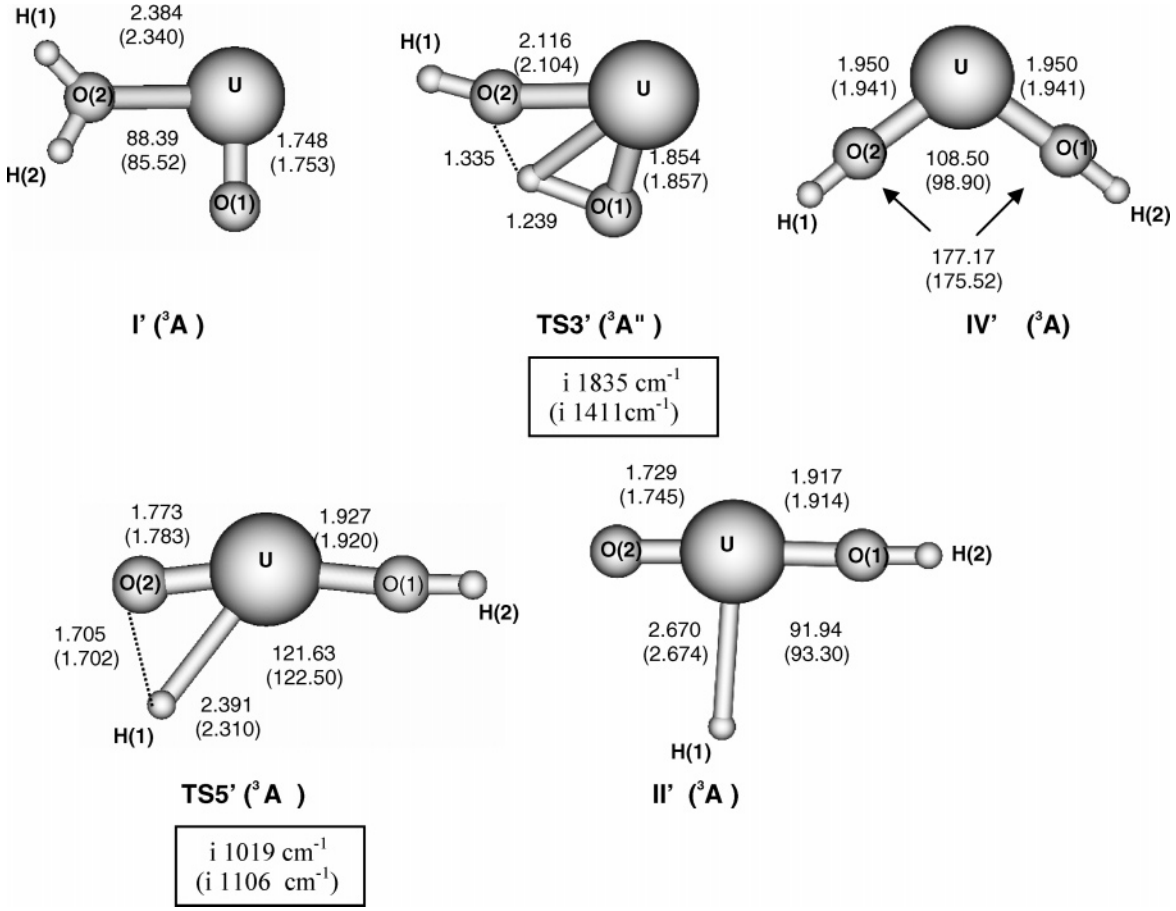


***Figure 8.*** Geometrical parameters of all the minima and transition states (lowest-energy spin state species) involved in the reaction of $UO^{2+}$ with $H_2O$ (Path B), at the B3LYP/SDD and PW91/ZORA levels of theory (in parentheses). Bond lengths are in Ångstroms, and angles are in degrees.

methodologies and to unravel the energetical differences obtained from different DFT approaches would be to perform advanced ab initio methods, with the cost factor implied.

**Bonding Analysis.** As previously mentioned, the bonding properties of all the species involved in the studied reaction pathways were investigated by using three different metodologies. In particular, we have analyzed the topological properties of the ELF function, the AIM analysis, and the more traditional NBO approach. The details of that analyses are included in the Supporting Information of this paper, whereas in this section we summarize the main conclusions drawn from that study.

(1) The main characteristic of the U−O bonds present in the structures under study is their high ionic character. In ELF analysis, this is evidenced by the presence of a disynaptic valence basin betwen the U and O atoms, with a very high electronic population (around 7 electrons), in which the contribution of U atom to the total basin population is always very low, usually between 3 and 10%.

(2) An analysis of the bond critical points (bcp) of the gradient vector field of the charge density (AIM analysis) indicates that the U−O bonds are characterized by values of $\rho$(bcp) that are usually around 0.30 a.u., whereas the Laplacian at the bcp are always positive. Therefore, although $\rho$(bcp) is quite large, the Laplacian at the bcp is positive, indicating that charge density is concentrated in the separated atomic basins rather than in the internuclear region, which is thus locally depleted of electronic charge. Within AIM framework, such an interaction is usually considered as intermediate between shared and closed-shell interactions.

(3) We have performed NPA analysis by using two different atomic orbital partitions, the default partition of Gaussian03 code and a modified partition that includes the 6d orbitals into the valence space rather than in the Rydberg space. The inclusion of 6d orbitals in the valence space provokes an important lowering of the positive charges on the metal atom. Indeed, when using the default partition, those values are systematically higher than the AIM metal charges, whereas with the modified partition, the values are in all cases lower than those values. The qualitative picture of the bonding provided by ELF and AIM analysis is not contradicted by the NBO analysis. The polarization coefficients of the NBO formed between U and O atoms indicate that the main contribution to that MOs comes from O atom (around 70−80%).

## Conclusions

From the above presented results, we can conclude that the major channel for the reaction of the mono- and dicationic uranium monoxides with water is the $H_2$ elimination. This result fully agrees with the low-pressure FTICR−MS experiments and puts in evidence that the different results obtained from high-pressure QIT−MS experiments are a consequence of the three-body processes that take place, which enable the dissociation of the first insertion intermediate, $H-UO_2H^+$, to $UO_2H^+ + H$. A comparison between the dehydrogenation pathways clearly shows that the reaction profiles are quite different and that the

reaction of $UO^+$ is largely favored, both thermodynamically and kinetically. The reaction of the single charged monoxide is very exothermic (around 276 kJ/mol at the B3LYP/SDD level). From BDEs values (Table 1) and considering the $H_2-O$ BDE (491 kJ/mol), the formation of the monocationic dioxide concomitantly with the loss of molecular hydrogen is expected to be exothermic by 280 kJ/mol. The theoretically predicted reaction barriers were found to be well below the $UO^+ + H_2O$ dissociation limit.

The dehydrogenation process may proceed by two different mechanisms; in the first one, the hydrido-metal-hydroxy intermediate is directly formed from the initial ion−molecule complex, via the first transition state. This pathway (Path A) involves two transition states. The second mechanism instead includes a preliminary formation of a very stable bis-hydroxide intermediate (Path B), which is formed from the same initial $UO^+-H_2O$ moiety. From this intermediate, the system has to surpass a second transition state to form the hydrido-metal-hydroxy intermediate so the $H_2$ elimination channel evolves. The reaction barrier associated to this process is very high, namely, almost two times the energetical barrier for the direct formation of $H-UO_2H^+$ from the initial ion−molecule complex. In both cases (Paths A and B), the crossing between the surfaces takes place just before the formation of the hydrido-metal-hydroxy moiety, and from that point of the reaction, there is a progressive stabilization of the insertion intermediates.

The reaction of the dicationic oxide is much less exothermic (almost 12 kJ/mol at the B3LYP/SDD level). From BDEs (Table 1), that value is predicted to be of around 68 kJ/mol. There is a very strong stabilization of the first ion−molecule complex, much higher than the corresponding $UO^+-H_2O$ complex, whereas the first insertion intermediate is very high in energy (at the B3LYP/SDD level, this structure is even over the reactants limit). In this reaction, the crossing between the surfaces takes place after the formation of the $H-UO_2H^{2+}$ intermediate. The reaction barriers are more than two times the corresponding values for the $UO^+ + H_2O$ reaction. The barrier heights for the formation of the hydrido-metal-hydroxy intermediate for both mechanisms (Path A and B) are comparable.

A comparison between the $UO^+ + H_2O$ reaction with the previously studied $U^+ + H_2O$ path[7] shows that the exothermicity of the reactions can be considered comparable. For the reaction of the bare cation, the whole process evolves along the quartet ground spin state of $U^+$, whereas the $UO^+ + H_2O$ reaction is a multistate process. The barrier height for the direct formation of the hydrido-metal-hydroxy intermediate is more than double that of the same barrier for $U^+ + H_2O$ reaction. In contrast, as a consequence of the higher stabilization of the first insertion intermediate of the $U^+ + H_2O$ reaction ($H-UOH^+$), the second reaction barrier for the $UO^+ + H_2O$ reaction is almost half of the corresponding value for the $U^+$ reaction. The dissociation barrier is much lower in the $UO^+ + H_2O$ reaction, with some disparity in the amount of the decrease, depending on the theoretical level.

The exothermicity of the $UO^{2+}$ and $H_2O$ reaction is much lower than the corresponding value for the bare cation reaction.[7] We note of that of all the studied reactions (bare and monooxides uranium cations), this is the only case in which the reaction barriers are predicted to be well above the dissociation limit of $UO^{2+} + H_2O$. Our calculations indicate that the transition barriers for the formation of the hydrido-metal-hydroxy intermediates are notably higher than the corresponding value for the $U^{2+} + H_2O$ path, whereas the value of the second barrier (formation of the dihydrogen-intermediate) can be considered comparable. The values of the dissociation barriers are comparable for both reactions.

In conclusion, the calculations presented in this paper confirm the hypothesis that the reaction of $UO^{2+}$ with water is not experimentally detected owing to its slowness.

In the case of the $UO^{+(2+)} + H_2O$ reactions, the rate-limiting step is the formation of the hydrido-metal-hydroxy intermediate. For the bare cation reactions instead, the rate-limiting step is the second step (formation of the $(H_2)UO^+$ intermediate) for $U^+$, whereas for the reaction of $U^{2+} + H_2O$, the barrier heights are comparable.

**Acknowledgment.** Financial support from the Università degli Studi della Calabria is gratefully acknowledged.

**Supporting Information Available:** Complete reference 14. Bonding analysis (ELF, AIM, and NBO) of all the minima and transition states involved in the studied reaction pathways. This material is available free of charge via the Internet at http://pubs.acs.org.

JA065683I